On the effect of plastic model on simulation of adhesive bonded joints with FM94

Quan, H.; Alderliesten, René

DOI
10.1016/j.ijadhadh.2021.102916

Publication date
2021

Document Version
Final published version

Published in
International Journal of Adhesion and Adhesives

International Journal of Adhesion & Adhesives 110 (2021) 102916

Contents lists available at ScienceDirect

International Journal of Adhesion and Adhesives

journal homepage: www.elsevier.com/locate/ijadhadh

On the effect of plastic model on simulation of adhesive bonded joints with FM94

H. Quan *, René Alderliesten

Structural Integrity & Composites, Faculty of Aerospace Engineering, TU Delft, Netherlands

ARTICLE INFO

Keywords:
FM94 property
Adhesive joint simulation
Plastic model

ABSTRACT

The stress-strain relationship of adhesive material is important as an input for numerical simulation. In this paper, a series of quasi-static experiments to measure the stress-strain relationship of FM94 adhesive material is reported. The experiments include the bulk tension test to obtain the tensile property and the V-notched beam shear test to obtain the shear property. The FE simulation with the Drucker–Prager model shows good agreement with experimental results. Moreover, further numerical results of adhesive joints show it is not always proper to use the Von Mises model to simulate adhesive joints as some previous studies proposed. The experimental results clearly show that the effective yield stress of adhesive materials is different for tension and shear, which disagrees with the Von Mises model often adopted in simulation.

1. Introduction

The adhesive joint is one of the main joining methods in industrial practice. From the view of research and design, it is important to predict the behaviour of adhesive bonding under unknown/unanticipated service conditions. For a reliable methodology to analyze adhesive bonding, detailed material properties of adhesive materials, for example the stress-strain relationship, damage models and failure criteria, are necessary to fully capture the material behavior in structures.

FM94 is a typical epoxy film adhesive from Cytec/Solvay, which currently is used in aerospace. FM94 is used together with S-glass fibre in GLARE, which is used in A380's fuselage. For both numerical simulation of adhesive joints and some simple calculation to check the structural integrity during structural design in A380, the stress-strain relationship of FM94 is an important input, because it shows the mechanical behaviour of this adhesive material.

Measuring the stress-strain relationship of adhesive materials is a mature area. This is illustrated by the studies [1–6] presenting experimental methods to measure the stress-strain relationship of adhesive materials. Among them, the test standards [4–6] provide detailed and practical instructions for conducting experiments and data processing.

Similarly, there is quite some work reported on both numerical simulations and analytical solutions [7–21], where suitable constitutive models, often including plasticity, are needed to accurately reproduce the material property measured from experiments. Some of the studies, i.e. [7–11], used the Von Mises model to simulate the plastic behaviour of adhesive materials in adhesively bonded structures, because this model is simple. For the Von Mises model, only the Poisson's ratio and either tensile or shear stress-strain curve are needed.

However, some experimental results [1,2] clearly show that the effective yield stress at a certain effective plastic strain of adhesive materials changes with hydrostatic pressure rather than remaining constant. The Von Mises model ignores the effect of hydrostatic pressure on the yield stress, thus limiting its applicability for describing the plastic behaviour of adhesive materials observed in experiments.

Fortunately, there have already been some successful attempts to overcome this problem. García [2], Dean [12], Zgoul [13] and Özer [14] used the Drucker–Prager plastic model in their studies to describe the variation of yield stress with hydrostatic pressure. As an alternative to the Drucker–Prager model, an anisotropic plastic material model by Castro [15] and the Raghava plastic model [16] were proposed respectively to describe the variation of yield stress with hydrostatic pressure in adhesive materials.

Nevertheless, when it comes to the study of crack within the adhesive bonded joint (for example, as with the DCB specimen for Mode I crack growth) [17–21], surprisingly some researchers still simulate adhesive materials with the Von Mises model. For example, Jokinen [17], Ameli [18], Azari [19], Donough [20] and Pascoe [21] studied the adhesive joints containing a crack using the Von Mises model. However, the stress field is complex and often in triaxial condition in the crack tip vicinity.

* Corresponding author. Room 0.38, Kluyverweg 1, 2629HS, Delft, Netherlands.
E-mail address: h.quan@tudelft.nl (H. Quan).

https://doi.org/10.1016/j.ijadhadh.2021.102916
Received 3 May 2021; Accepted 22 May 2021
Available online 1 June 2021

For example around the crack tip in DCB specimens, the adhesive material has stress in the plane of beam bending, meanwhile the transverse stress perpendicular to the plane of beam bending exists inside the adhesive layer. Therefore, these numerical results using the Von Mises model are not expected to be fully correct, for the effect of hydrostatic pressure on yield stress is ignored.

In this paper the differences in numerical results caused by different plastic models (the Von Mises model and the Drucker–Prager model) for adhesive materials are compared and discussed. First, to obtain the parameters in each model and validate each model, experiments are reported where the stress-strain relationship of the FM94 adhesive under tension and shear were measured. Second, several relevant numerical cases are used to demonstrate the difference between the Von Mises model and the Drucker–Prager model, and to discuss the influence of this difference on numerical results in general.

2. Experimental methodology and results

The experimental work includes the bulk tensile test and the V-notched beam shear test, to measure the stress-strain relationship under tension and shear respectively. The geometry of the specimens follows ASTM standard D638 for tension and ASTM standard D5379 for shear, as illustrated in Fig. 1.

2.1. Specimen manufacturing and preparation

The specimen manufacture was divided into two steps. First an adhesive plate was manufactured, which in a second step was cut into specimens with the required geometry.

In order to manufacture the plate from the film adhesive while controlling the thickness and shape of the plate, two mold plates together with four spacers were used, as illustrated in Fig. 2.

The film adhesive was cut into rectangles of 360 by 180 mm, the intended dimensions of the adhesive plate and stacked layer by layer in sequence. The stacked film adhesive was surrounded by four spacers with the thickness equal to the designed thickness of the plate. The spacers for manufacturing the plate for tensile specimens were 2.5 mm thick, and the spacers for manufacturing the plate for shear specimens were 4 mm. A release agent was applied on the contact surface of the two mold plates and to all the surfaces of the spacers, to enable easy release of the adhesive plate from both mold plates and spacers after curing.

During the manufacturing, one potential problem is associated to entrapped air creating bubbles during curing, which results in voids and defects in the final plate. To avoid this problem, every time after applying 3 layers of film adhesive, the lower mold plate and applied adhesive layers were fully vacuumed in a sealed vacuum bag and kept in 10 min to get rid of the air between layers. After applying all film adhesive layers, the total thickness of all the stacked adhesive layers was 0.5 mm larger than the thickness of the four surrounding spacers. That guaranteed the volume of the adhesive material to be larger than the volume of the space enclosed by the two mold plates and four spacers.

Before curing in the autoclave, all the stacked film adhesive layers together with two mold plates and four spacers were vacuum bagged, as shown in Fig. 3. The curing procedure followed the instruction by the supplier. During curing, firstly the temperature was raised from 24 °C to 121 °C in 50 min, and then the 121 °C was maintained for 1 h. Finally, the temperature was cooled down to 24 °C in 50 min. The pressure during curing is 0.28 MPa. The adhesive plate obtained after curing is shown in Fig. 3(b).

In the second manufacturing step, the adhesive plates were mechanically cut without liquid to the dimensions of the designed specimens. Before testing, all the cutting edges were carefully polishing manually with very smooth SiC gridding paper with 30 μm grain size in order to eliminate the potential defects caused by machine cutting.

2.2. Test procedure and results

The FM94 adhesive material was tested both under quasi-static tension and shear conditions. The tensile tests were performed with a Zwick 20 KN tensile/compression machine with pneumatic grips as shown in Fig. 4(a). During the tests, a Vic-3D Digital Image Correlation (DIC) system with a pair of 80 mm lenses and 50Mpix cameras was used to measure the strain field in an approximate 40 mm by 32 mm region. The axial and transverse strain were measured by a group of “Virtual” extensometers, which is a function of the Vic-3D DIC post-processing software, as illustrated in Fig. 4(c).

The V-notched beam shear tests were performed also with the same Zwick machine, but with different clamping as shown in Fig. 4(b). During these tests, the strain field was monitored with the same DIC device in an approximate 35 mm by 28 mm region. The shear strain was calculated by summing the absolute values of elongation/shrinkage of the two “Virtual” extensometers, as in Fig. 4 (d). These “virtual” extensometers in the Vic-3D DIC post-processing software were with the same length and at same location as the strain gauges described in ASTM standard D5379 in +45° and −45° direction.

The experimental curves obtained with the quasi-static tensile and shear tests are given in Fig. 5. In this figure, both the tensile and shear stress-strain data was obtained by 7 specimens.

3. Simulation of material properties

The stress state in engineering structures is generally more complex than the adopted test conditions. To describe the material property in numerical analysis of engineering structures, a proper material model is needed to transfer the simple test stress condition to more complex stress state in real structure. The simulations were done with Abaqus 2017 standard. Considering the effect of hydrostatic pressure on yield stress, the Drucker–Prager model was used in simulation to reproduce the experiment for it is more popular among researchers [2,12–14] than the models by Castro [15] and Raghava [16]. Two versions of Drucker–Prager model were used here: the linear Drucker–Prager model and the exponent Drucker-Prager model.

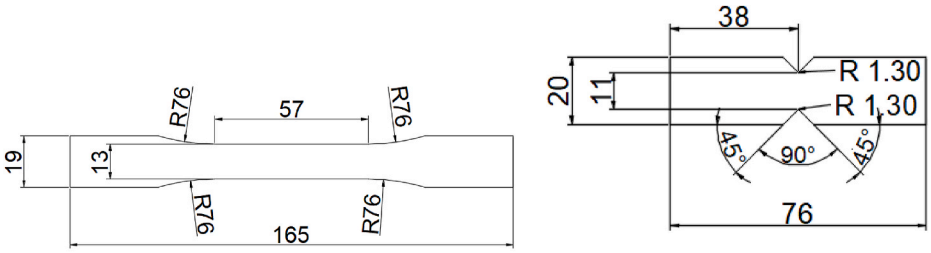

Fig. 1. The geometry of specimens:(a) Bulk tensile specimens; (b)V-notched shear specimens.

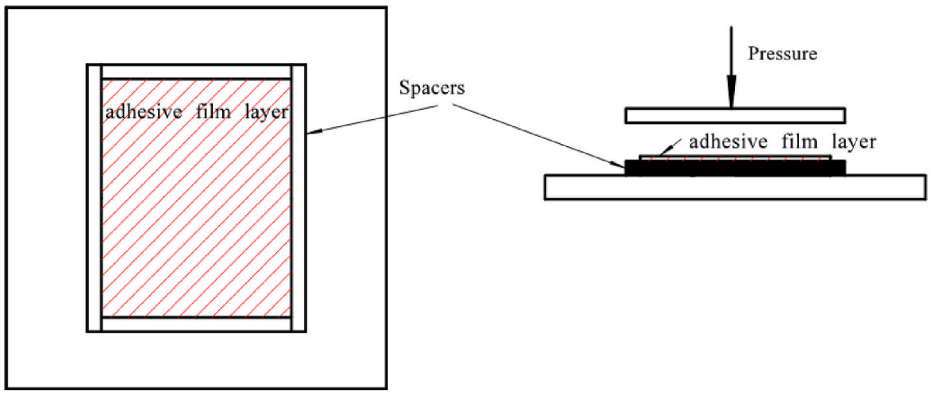

Fig. 2. Manufacturing method of adhesive plate with 4 spacers.

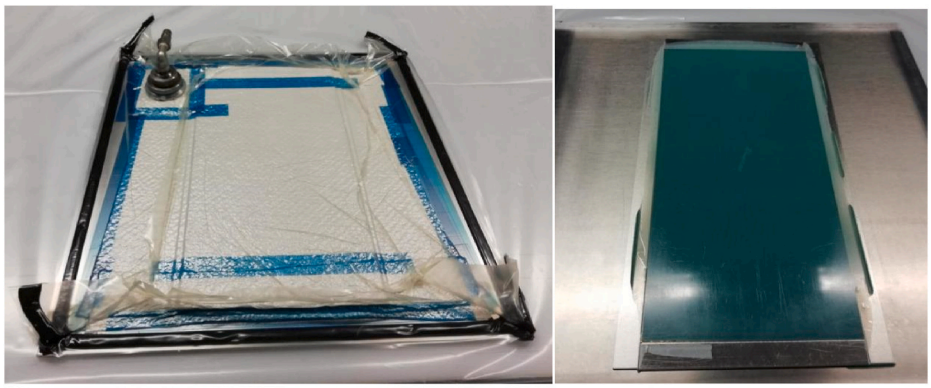

(a) The vacuum bagged plate before curing (b) The adhesive plate after curing

Fig. 3. Plate manufacture.

The yield criterion of the linear Drucker–Prager model is described as:

$$\sigma_e + \sigma_m \mu - \sqrt{3}\sigma_s = 0 \tag{1}$$

In this equation, σ_e is the Von Mises effective stress, σ_m is the hydrostatic pressure, μ is the material property accounting for the effect of hydrostatic pressure on yield stress and σ_s is the yield stress under shear.

Alternatively, in Refs. [1,2,12–14], an exponent Drucker-Prager model was used to simulate the stress-strain relationship of adhesive material:

$$a\sigma_e^b + \sigma_m - p_t = 0 \tag{2}$$

where a is a material parameter accounting for the effect of hydrostatic pressure on yield stress, and b is the exponent. p_t is the parameter representing hydrostatic tension strength.

3.1. Material parameters determination

For simulation, one important aspect is to obtain the material parameters that Abaqus requires. Before obtaining the material parameters, the engineering stress and strain (both in longitudinal and transverse direction) measured in tensile test were transferred into true stress and strain with Equations (3) and (4).

$$\varepsilon_{true} = \ln\left(1 + \varepsilon_{engineering}\right) \tag{3}$$

$$\sigma_{true} = \frac{\sigma_{engineering}}{\left(1 - \varepsilon_{engineering}\nu_{engineering}\right)^2} \tag{4}$$

where $\nu_{engineering}$ is the engineering Poisson's ratio obtained from the ratio of engineering transverse strain to longitudinal strain. Then the material data for elasticity, plastic yielding and plastic flow were obtained as the following procedure.

3.1.1. Elasticity

The elastic modulus and elastic Poisson's ratio were obtained from strain range of 0.0005–0.0025 in tensile data. The elastic Poisson's ratio was obtained from the ratio of transverse strain to longitudinal strain in tensile test. The elastic modulus $E = 2355.4$ MPa and elastic Poisson's ratio $\nu_e = 0.4$.

3.1.2. Plastic yielding

The plastic yielding parameters include both the parameters μ, a, b and p_t in Equations (1) and (2), and also the plastic hardening parameters to determine the hardening curve. The value of μ in Equation (1) was determined by the tensile yield stress σ_t and shear yield stress σ_s corresponding to the same effective plastic strain ε_e^p:

$$\mu = 3\left(\frac{\sqrt{3}\sigma_s}{\sigma_t} - 1\right) \tag{5}$$

$$\varepsilon_e^p = \frac{2}{3}\varepsilon_t^p\left(1 + \nu_p\right) = \frac{\gamma_p}{\sqrt{3}} \tag{6}$$

where ε_t^p and γ_p are the tensile longitudinal plastic strain and shear plastic strain respectively. The plastic component of the Poisson's ratio ν_p is determined by the ratio of the plastic part of transverse strain to

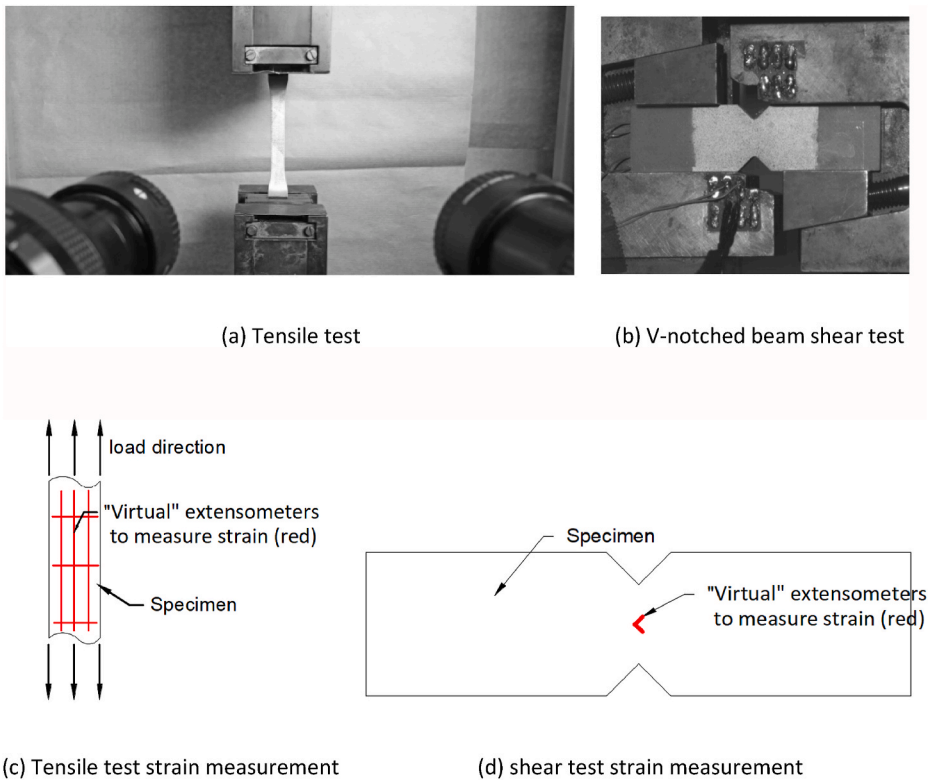

Fig. 4. Image of test and strain measurement illustration.

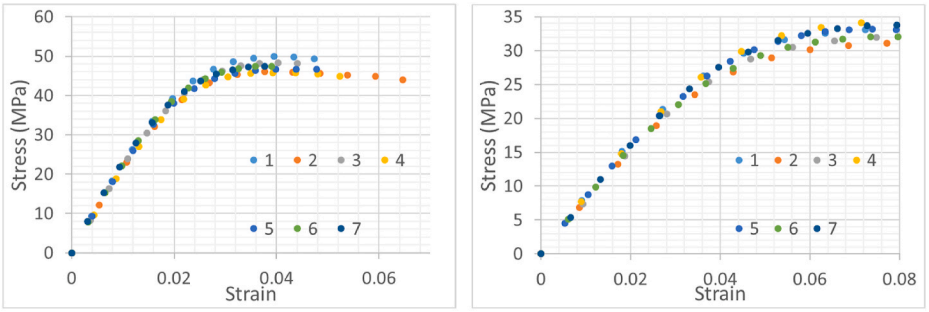

Fig. 5. Experimental engineering stress-strain data for FM94.

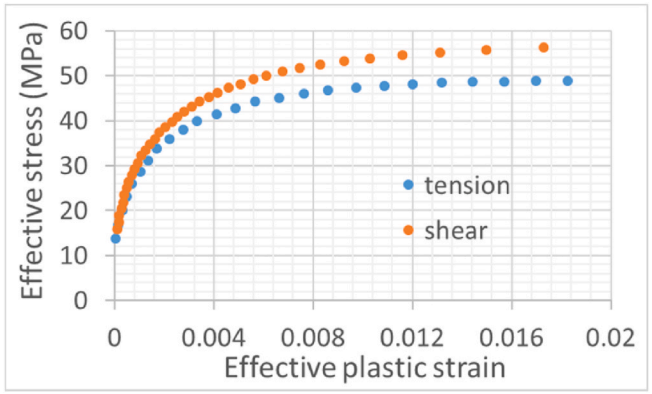

Fig. 6. The von Mises effective stress against effective plastic strain.

longitudinal strain. The von Mises effective stress for tension (σ_t) and shear ($\sqrt{3}\sigma_s$) against effective plastic strain ε_e^p are given in Fig. 6.

For the exponent Drucker-Prager model, a, b and p_t should be obtained. Unfortunately, the data from two test conditions (tension and shear) is insufficient to obtain 3 parameters. So an exponent Drucker-Prager model with the exponent equal to 2 was used as [1,2,12–14] for approximation. Then the exponent Drucker-Prager model becomes:

$$a\sigma_e^2 + \sigma_m - 3a\sigma_s^2 = 0 \tag{7}$$

The value of a was calculated using the tensile yield stress σ_t and shear yield stress σ_s corresponding to the same effective plastic strain ε_e^p:

$$a = \frac{\sigma_t}{3\left(3\sigma_s^2 - \sigma_t^2\right)} \tag{8}$$

Therefore, the parameters in the Drucker-Prager model in Equations (1) and (2) are $\mu = 0.456$, $a = 0.021(\mathrm{mm}^2/\mathrm{N})$, $b = 2$ and $p_t = 3a\sigma_s^2$.

The plastic hardening parameters are input in a form of direct tabular

data with the true stress and corresponding true plastic strain obtained from the plastic part of tensile stress-strain curve.

3.1.3. Plastic flow

Parameters for plastic flow are needed to account for the non-associated flow. The plastic component of the Poisson's ratio ν_p, determined by the ratio of the plastic part of transverse strain to longitudinal strain, is not 0.5 as in the Von Mises model. In ABAQUS, the dilation angle ψ from the flow potential is used for describing this behavior. The value of ψ can be calculated with [1,2]:

$$\tan\psi = \frac{3(1-2\nu_p)}{2(1+\nu_p)} \tag{9}$$

The value of ν_p is 0.35 and the value of ψ is 18.43°.

3.2. Comparison between simulation results and experimental data

The simulation of FM94 under pure tension and pure shear was conducted with the linear Drucker–Prager model (DPL), the exponent Drucker-Prager model (DPE), the Von Mises model with tensile data (VMT), and the Von Mises model with shear data (VMS). The comparison of simulation results and test data presented in Fig. 5 is shown in Fig. 7. In Fig. 7(a) the results of DPL, DPE and VMT fall onto the same line, because DPL, DPE and VMT use the same tensile plastic hardening direct tabular data as input. In Fig. 7(b) the simulation result of pure shear with VMS is not given because the parameters of VMS are directly from the shear test data and the simulation fits perfectly with test data.

From Fig. 7, it is concluded that both the linear Drucker–Prager model and the exponent Drucker-Prager model can reproduce both the tensile and shear stress-strain relationship of FM94 very well. However, the Von Mises model only fits tensile test data when used with tensile input data and only fits shear test data when using shear input data. The Von Mises model does not fit both load conditions, for it ignores the effect of hydrostatic pressure on yielding.

4. Numerical case studies with adhesive bonded joints

In this section, 4 examples of the commonly used engineering structures under complex stress condition in reality were studied, including: 1. single lap adhesive bonded joints, 2. plate with cutout reinforced by doublers, 3. crack in adhesively bonded joints and 4. plate with crack bonded repaired. Those examples are given with the FM94 experimental data to demonstrate the difference in numerical results caused by different material models.

The numerical simulation was done with both the Von Mises model (VMT and VMS) and with the linear Drucker-Prager model (DPL). The exponent Drucker-Prager model (DPE) was not used in further simulations for 2 reasons. First unlike DPL, whose parameters were all obtained accurately from current test data, the parameter $b = 2$ in DPE was approximately obtained from literature [1,2,12–14] on other adhesive materials, instead of the current test data, for the current test data is insufficient to obtain all the parameters in DPE. Second DPL has better convergence than DPE in ABAQUS.

For each simulation example, the whole finite element models are perfectly the same, except for the material property of the adhesive layer. The simulation results with DPL were considered as the reference to verify the simulation results with VMT and VMS, because the linear Drucker-Prager model fits the test data in both tensile and shear condition well, unlike the Von Mises model. The VMT fails in shear test data and the VMS fails in tensile test data.

4.1. Single lap adhesive bonded joints under tension

The first example is the simulation of a single lap joint, as illustrated in Fig. 8, which is commonly applied as a standard test method in evaluating bonding quality. Three models were simulated in this example, the overlap length and adherend thickness of each model are given in Table 1. The geometry of Model #1 follows ASTM standard D1002. The geometry of Model #2 has the same overlap with Model #1 but larger thickness(3 mm). A larger thickness was chosen to increase the bending of single lap joints, but 3 mm has no specific reason, just providing an example to see the trend. The geometry of Model #3 has the same thickness with Model #2 but shorter overlap(9 mm), making the bending of single lap joints increasing monotonically from #1 to #3. Again 9 mm overlap has no specific reason, just providing an example to see the trend. The adhesive material in the joints is mainly dominated by shear force. However, with the bending taking place because of the misalignment of the loading on both adherents, the adhesive material in the joints also experiences peeling. This could result in an inaccuracy particularly when using the Von Mises model in simulations. From #1 to #3 in Table 1, the bending keeps increasing.

The numerical simulation was performed with 3D FEA in Abaqus. The element used is 8-node reduced integration element, with enhanced hourglass control. The adherend material is aluminum alloy with elastic modulus 69.2 GPa and Poisson's ratio 0.3. The nominal thickness of the adhesive layer is 0.15 mm, approximately representing 1 layer of film adhesive. The FEA model is from a whole part in ABAQUS contains both the aluminum material property and adhesive material property in the corresponding region. The adhesive material is meshed with $40 \times 30 \times 8$ elements in loading, width and thickness direction respectively to reach convergence in simulation results.

The boundary condition is shown in Fig. 8(b). One the left side, the displacement in X and Y direction are constrained. On the right side, the

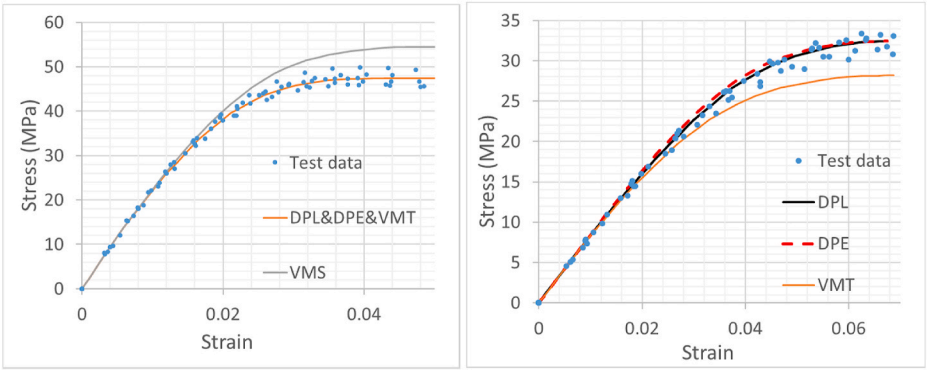

(a) Tension (b) Shear

Fig. 7. Comparison of engineering stress/strain between experimental data with simulation results.

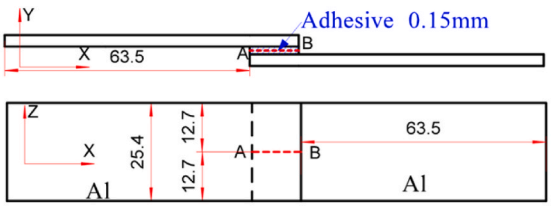

(a) Geometry

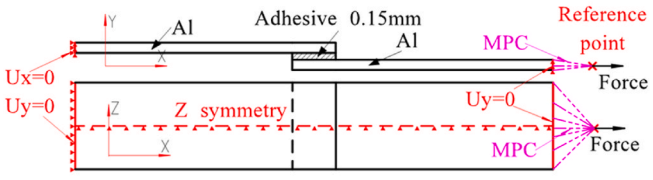

(b) Boundary condition

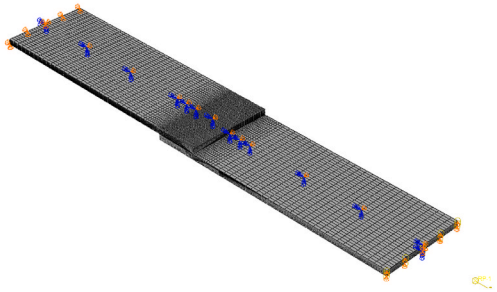

(c) Single lap FEA model with 1.6 mm thick adherends

Fig. 8. Single lap adhesive bonded joints.

Table 1
Overlap length and adherend thickness.

Model number	Overlap length (mm)	Adherend thickness (mm)
#1	12.7	1.6
#2	12.7	3
#3	9	3

displacement in Y direction is constrained. An MPC constraint is used between the right side and a reference point, keeping the same displacement in X direction. The load is applied on the reference point. A symmetrical boundary condition in Z direction is in the middle width plane. The FE model with the 1.6 mm thick adherend is shown in Fig. 8 (c). The FEA was performed with ABAQUS standard with nonlinear geometry on.

The shear stress in path A-B in Fig. 8, which is at the mid-plane of the bond-line, was chosen for comparison. The resulting stress distributions corresponding to 5 KN load over path A-B are shown in Fig. 9. The x-axis representing the distance to Point A was normalized, with Point A to be 0 and Point B to be 1 in x-axis. The numerical results with the linear Drucker-Prager model are close to the numerical results with both versions of the Von Mises model. The differences mainly occur in the region around the edges with high peeling stress corresponding to high hydraulic pressure.

For shear stress, VMS results has the largest maximal stress. The VMT and VMS have the same location of maximal stress. The distance between two points of maximal stress for DPL is closer than VMS and VMT. From #1 to #3, as the bending increases, the numerical results with DPL are closer to the VMT numerical results than the VMS results. This is attributed to the increasing bending causing the increasing peeling stress in the adhesive bonds. With the higher peeling stress, the DPL results become closer to the VMT results. For the peeling stress, the DPL results are closer to the VMT results. Therefore, for single lap adhesively bonded joints under tension either Von Mises model is suitable to obtain the shear stress in the bond-line, but when bending becomes more dominant, with decreasing overlap length or increasing adherend thickness, the Von Mises model with tensile data is recommended instead of the Von Mises model with shear data.

4.2. 2024-T3 plate with cutout reinforced by doublers

Cutouts are important in aircraft structure for maintenance and passing cables and fuels, so the second example is a 2024-T3 plate with round hole cutout and reinforced with 2 ring doublers (also 2024-T3) on both sides, as shown in Fig. 10. The inner and outer diameter of doublers are 76 mm and 100 mm. The plate is 2 mm thick and the doublers are 1 mm thick. The adhesive layer between plate and doubler is 0.15 mm thick, corresponding to one layer of adhesive. The stress-strain curve of 2024-T3 used is shown in Fig. 11. A cylindrical coordinate system *(r, θ, z)* with the origin to be the hole cutout center as in Fig. 10(a) is used for the convenience of presenting the numerical results later. The r-θ plane is parallel to the X-Y plane..

The FEA model is from a whole part in ABAQUS contains both 2024-T3 material property and adhesive material property in the corresponding region. The adhesive material is meshed with 25 × 200 × 6 elements in radius, circumferential and thickness direction respectively. The element is 8-node reduced integration element with enhanced hourglass control.

The boundary condition is shown in Fig. 10(b). A half model was used in simulation for the symmetrical boundary condition in Z direction. Displacement in X and Y direction are constrained in the left corner point on the symmetrical plane and displacement in Y direction is constrained in the right corner point to eliminate the rigid body motion. The model is subjected to normal stress in X direction σ_x, normal stress in Y direction σ_y, and shear stress in XY plane τ_{xy}, with the value $\sigma_x = \sigma_y = 2\tau_{xy} = 200$ MPa, for the loading conditions of aircraft structure are often under both tension and shear. The FEA was performed with ABAQUS standard with nonlinear geometry on. The 3D FEA model is shown in Fig. 10(c).

The stress and plastic strain distribution in the mid-plane of bond-line are used for comparison. Because the plasticity occurs first in the outer circle edge of the adhesive material, the simulation results of the circumferential normal stress $S_{\theta\theta}$, shear stress $S_{\theta z}$, circumferential normal plastic strain $\varepsilon^p_{\theta\theta}$ and shear plastic strain $\varepsilon^p_{\theta z}$ on the outer radius $r = 50$ mm in the mid-plane of bond-line are presented in Fig. 12.

It can be observed that, choosing different plastic models in simulation can give noticeable differences in numerical results. The normal stress and normal plastic strain with VMT are closer to the simulation results with DPL, conversely the shear stress and shear plastic strain with VMS are closer to the simulation results with DPL. The results with DPL are used as reference to verity the results with VMS and VMT as stated previously because DPL can fully reproduce the test data for both tension and shear, while the Von Mises model cannot. The numerical results with VMT and VMS show clear differences with the numerical results with DPL, so the Von Mises model cannot fully reproduce the stress and strain fields of adhesive materials under mixed tensile-shear loading condition. Because under mixed tensile-shear loading, the hydrostatic pressure influences the plastic behavior of adhesive materials, but the Von Mises model cannot take it into account.

4.3. Plastic dissipation in crack tip area

The third example comprises the simulation of a plastic zone and

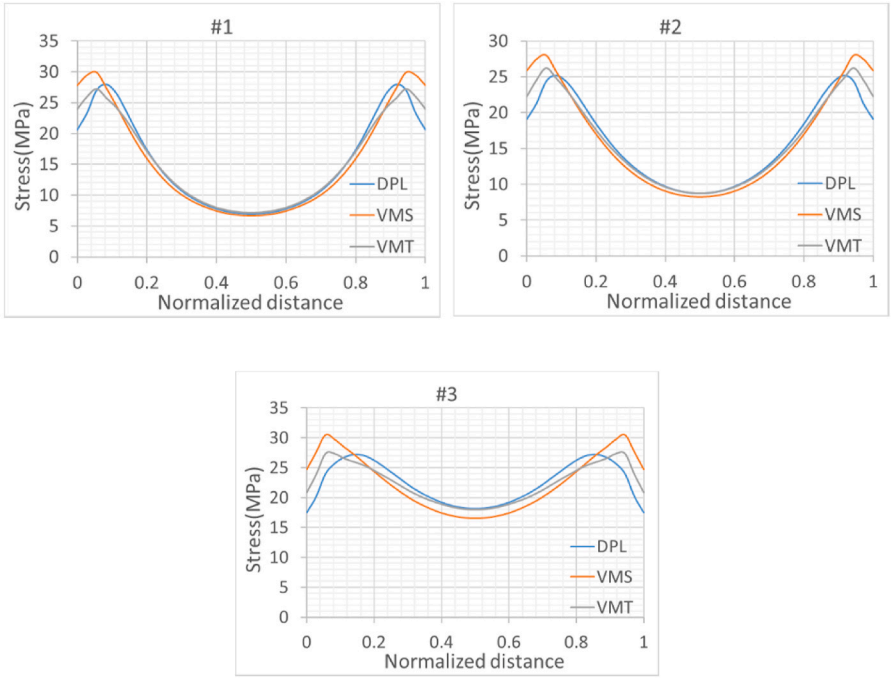

(a) Shear stress

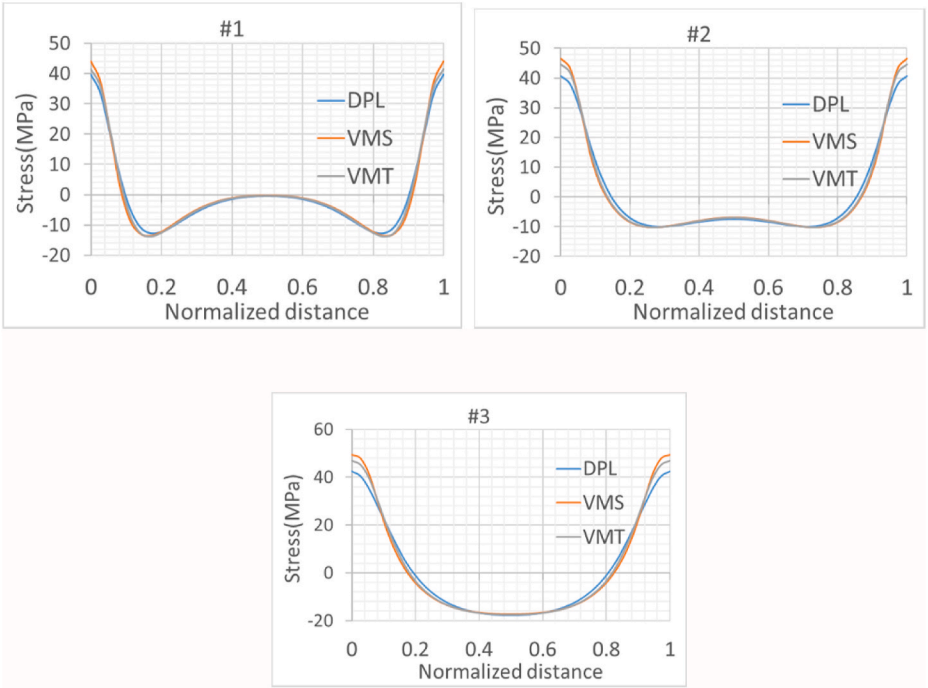

(b) Peeling stress

Fig. 9. Stress distribution at the mid-plane in the bond-line.

plastic dissipation around the crack inside the adhesive layers. Double Cantilever Beam (DCB) and End-notched flexure (ENF) specimens were simulated to illustrate the differences caused by different material models in Mode I and Mode II, respectively. The reason for selecting this example is that those specimens are widely used as standard test specimen geometry in scientific research. The plastic dissipation in adhesive material was chosen as one indicator for comparison in this example, because it is obtained from both stress field and plastic strain field in the plastic zone.

In the example, the adherend material is aluminum alloy with $E = 69.2$ MPa and $\nu = 0.3$. The geometry follows ASTM standard D5528 and D7905, for Mode I and Mode II respectively. The thickness of adhesive is

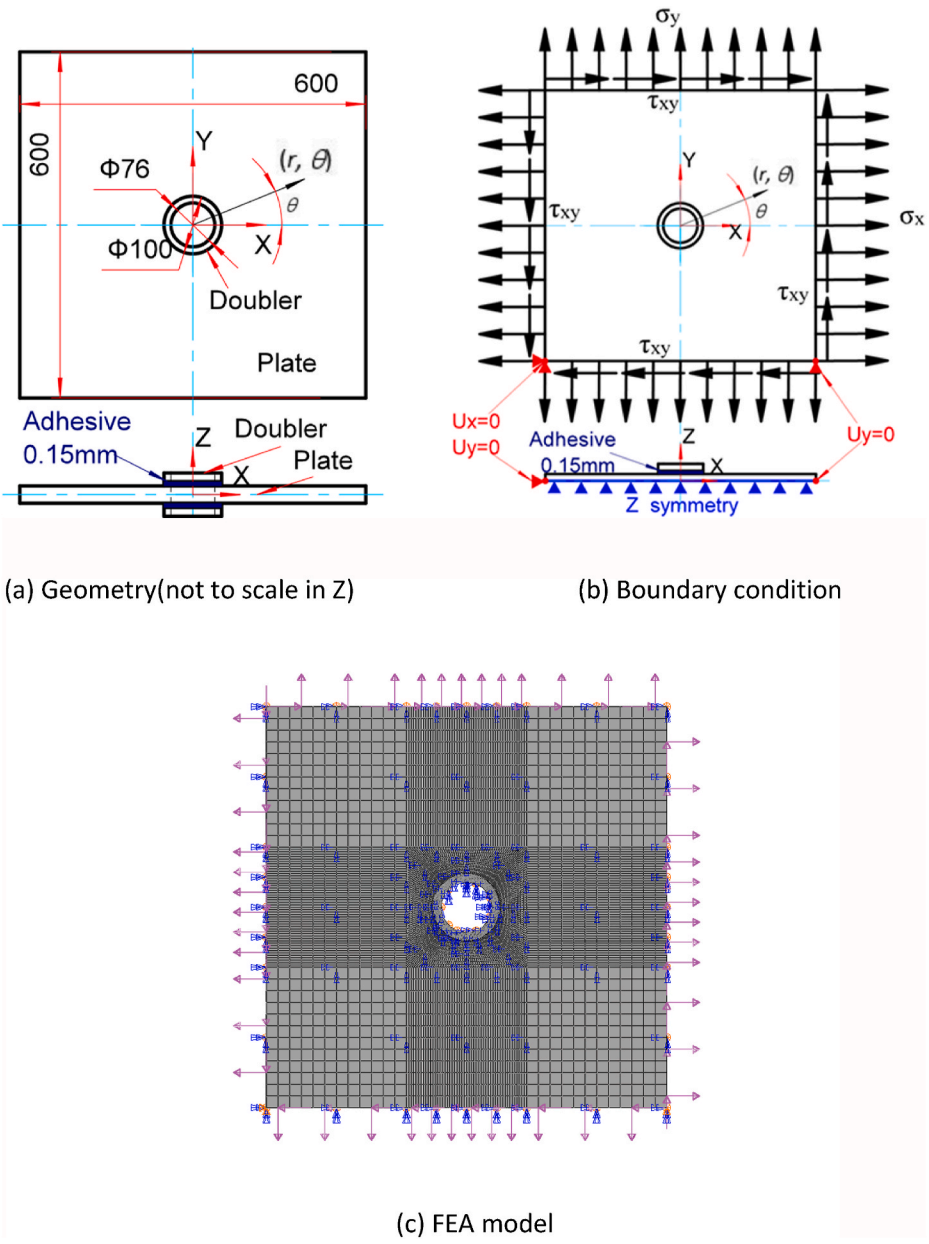

Fig. 10. Open hole plate with reinforcement

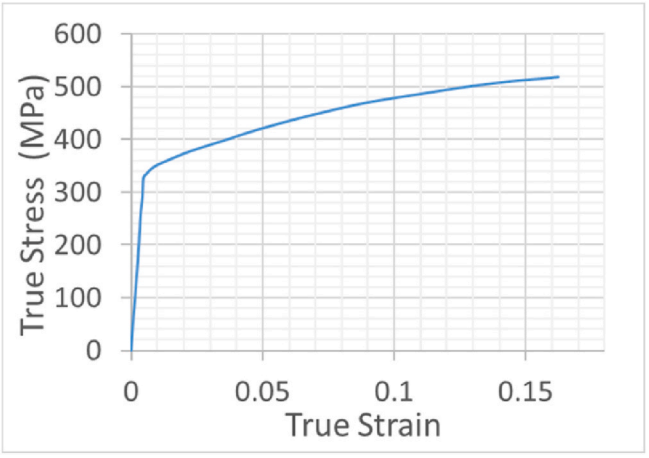

Fig. 11. Material properties of 2024-T3 used in simulation.

0.3 mm rather than 0.15 mm for giving a better illustration of plastic zone.

The DCB specimen was simulated in both 3D and 2D plane strain condition. The geometry and boundary condition are in Fig. 13. Both 2D and 3D models contain two separate parts containing both adherend and adhesive material properties. A Tie constraint is located in the region without crack, and two free surfaces represent the crack surface. The displacement in X and Y direction at the bottom left corner in X–Y plane are constrained, and the displacement in X direction at the top left corner in X–Y plane is constrained. An MPC constraint is used between the top left corner and a reference point, keeping the same displacement in Y direction. The load is applied on the reference point. A half model is used for the symmetrical boundary condition applied in Z direction for 3D model.

The DCB specimen was force controlled. The energy release rate was calculated with simple beam theory with Equation (10) [22]:

$$G_I = \frac{3P\delta}{2ab} \tag{10}$$

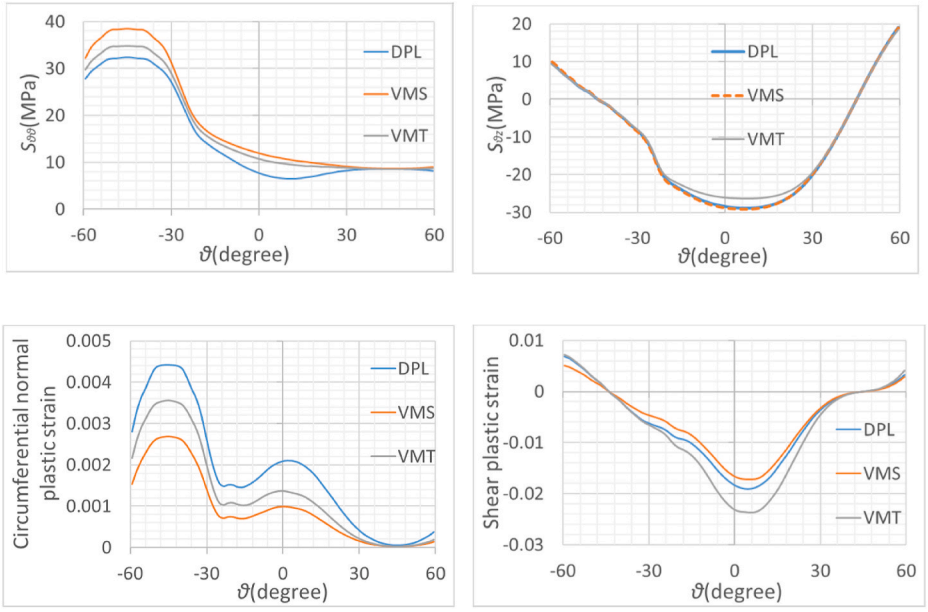

Fig. 12. FEA results of stress and plastic strain distribution.

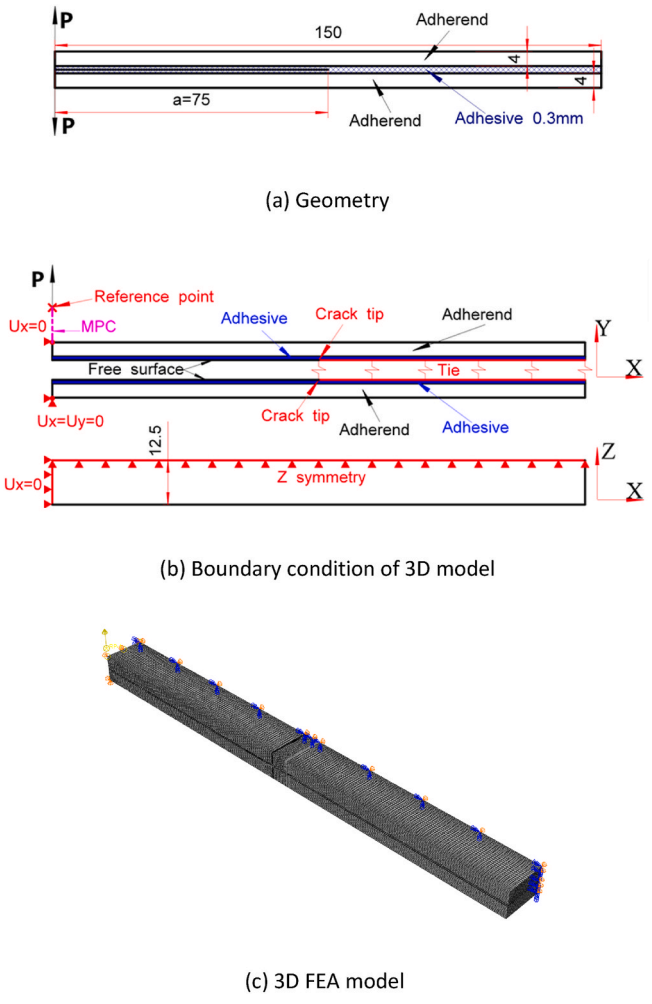

Fig. 13. Geometry and boundary condition of DCB specimen.

where P and δ are the load and opening displacement respectively. a is the crack length, and b is the width. The plastic dissipation E_{pl} was calculated by integration over the plastic zone V_{pl} in Equation (11):

$$E_{pl} = \int \sigma_{ij}\dot{\varepsilon}^{p}_{ij} dV_{pl} \tag{11}$$

where σ_{ij} and ε^{p}_{ij} are the stress and plastic strain respectively.

The plastic dissipation at different G_I is obtained by Abaqus history output, as shown in Fig. 14. It can be observed that the plastic dissipation with DPL is much higher than plastic dissipation with VMS and VMT for both 2D and 3D. The same trend of 2D and 3D numerical results should be attributed to the same mechanics occurring in both 2D and 3D simulation, which can be explained by comparing the plastic zone and plastic strain ahead of the crack tip in 2D model. The plastic zone with $G_I = 0.5$ N/mm is shown in Fig. 15, which illustrates that the plastic zone with DPL is much larger than the plastic zone with VMS and VMT.

The difference in size of plastic zone can be attributed to the different stress and strain fields caused by different material models. As Fig. 16 shows the Von Mises effective stress and plastic strain in Y direction ε^{p}_{yy} distribution in the mid-plane of bond-line ahead of the crack tip with $G_I = 0.5$ N/mm in 2D model. From the figure it could be observed that the Von Mises effective stress with DPL is much lower than Von Mises effective stress with VMS and VMT, while the plastic strain with DPL is much higher than plastic strain with VMS and VMT. The reason for this phenomenon is the high hydrostatic pressure ahead of the crack tip strongly influences the plastic yielding behavior of adhesive material. With a higher hydrostatic pressure, the Von Mises effective stress causing yielding becomes smaller with DPL, but the Von Mises effective stress causing yielding does not change with the Von Mises model. That explains lower Von Mises effective stress with DPL and larger plastic deformation in Fig. 16. Since the finite element models with DPL, VMS and VMT are perfectly the same except for the material property of the adhesive material, it is concluded that the Von Mises model is not suitable for the modeling of the plastic zone in the Mode I DCB adhesive joints for the adhesive material under consideration.

Besides, Fig. 16(a) also shows the simulation result of Von Mises effective stress with the finite element model with 0.15 mm thick adhesive layer and VMT to be the adhesive material property. When comparing this result with the equivalent 0.3 mm thick adhesive layer, it is observed that the Von Mises effective stress increases with decreasing

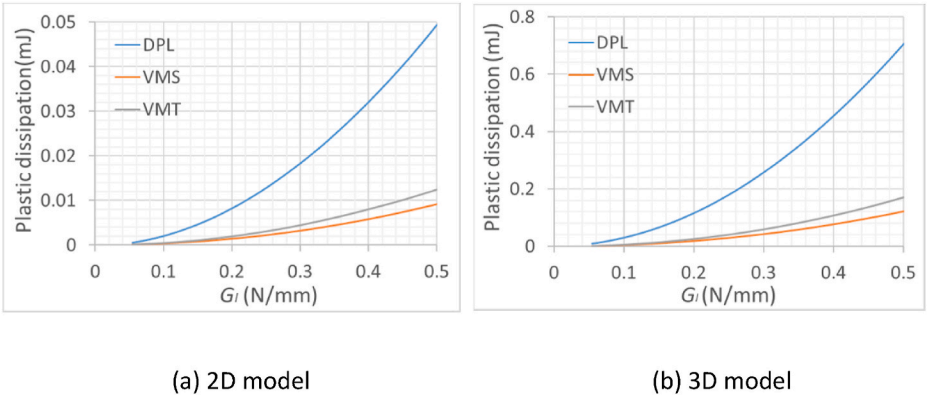

Fig. 14. Plastic dissipation of DCB specimen.

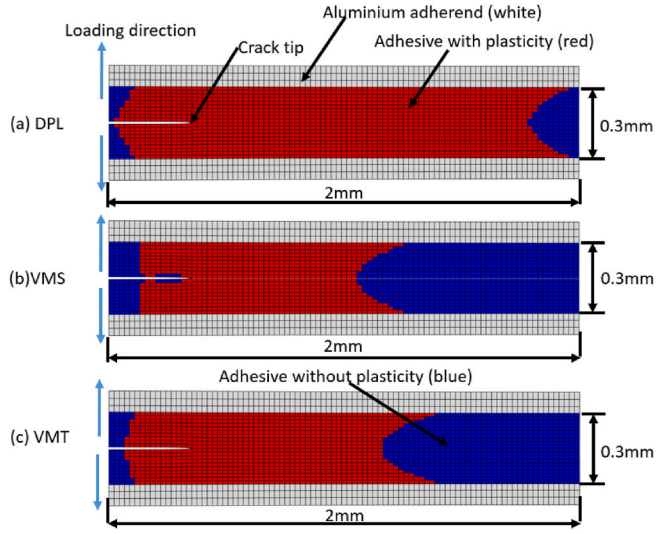

Fig. 15. FEA results of the plastic zone (red) size and shape for DCB specimen. (For interpretation of the references to colour in this figure legend, the reader is referred to the Web version of this article.)

adhesive thickness. This trend agrees with [19], making the simulation of this example more reliable.

The ENF specimen was simulated in both 3D and 2D plane strain condition. The geometry and boundary condition is in Fig. 17. The FEA models contain two separate parts containing different materials, and a Tie constraint is located in the region without crack. A surface to surface contact is set between two crack surfaces. The displacement in X and Y direction are constrained in the left roller position and the displacement in Y direction is constrained in the right roller position. An MPC constraint is used between the loading line and a reference point, keeping the same displacement in Y direction. The ENF specimen was force controlled, and the load is applied on the reference point.

The energy release rate was calculated by Ref. [22]:

$$G_{II} = \frac{9a^2 P\delta}{2b\left(2L^3 + 3a^3\right)} \tag{12}$$

where δ is the displacements and $L = 50$ mm is the half-span distance. The plastic dissipation is shown in Fig. 18. The Figure shows that the results with VMS is close to the results with DPL, while the results with VMT is higher than the other for both 2D and 3D model. It is unsurprising that the results with DPL is close to the results with VMS, for ahead of the crack tip the stress condition is close to pure shear in an ENF specimen. So, with almost zero hydrostatic pressure, the material property of DPL is close to VMS.

Again, the same trend of 2D and 3D numerical results should be attributed to the same mechanics occurring in both 2D and 3D simulation. The shear plastic strain ε_{xy}^{p} in the mid-plane of the bond-line ahead of the crack tip at $G_{II} = 0.03$ N/mm in 2D model is shown in Fig. 19. From Fig. 19, VMT tends to underestimate the effective stress in shear, causing larger plastic deformation than VMS. Therefore, for an ENF specimen with a pure Mode II crack, the Von Mises model with shear data is suitable for simulating the plastic zone in adhesive materials.

Therefore, the Von Mises model is not suitable for simulation of the plastic zone in the adhesive joint in Mode I, since the simulation results with DPL differs clearly with results obtained with the Von Mises model. However, when it comes to the Mode II ENF specimen where the load condition is close to pure shear around the crack tip, the Von Mises model with shear data should be considered as a better alternative.

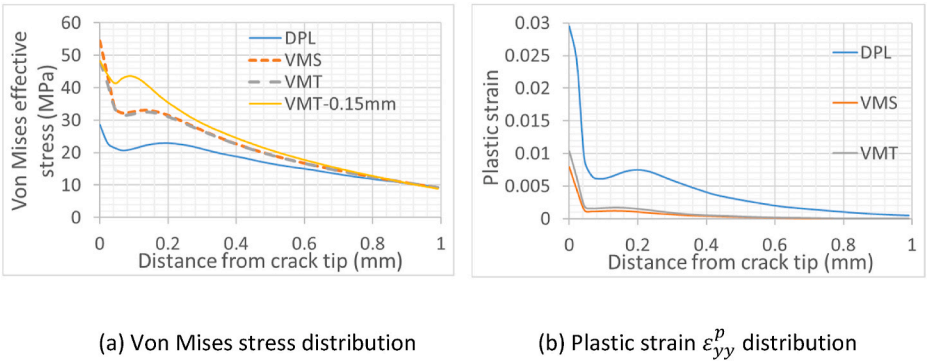

Fig. 16. Stress and strain distribution ahead of crack tip in 2D model.

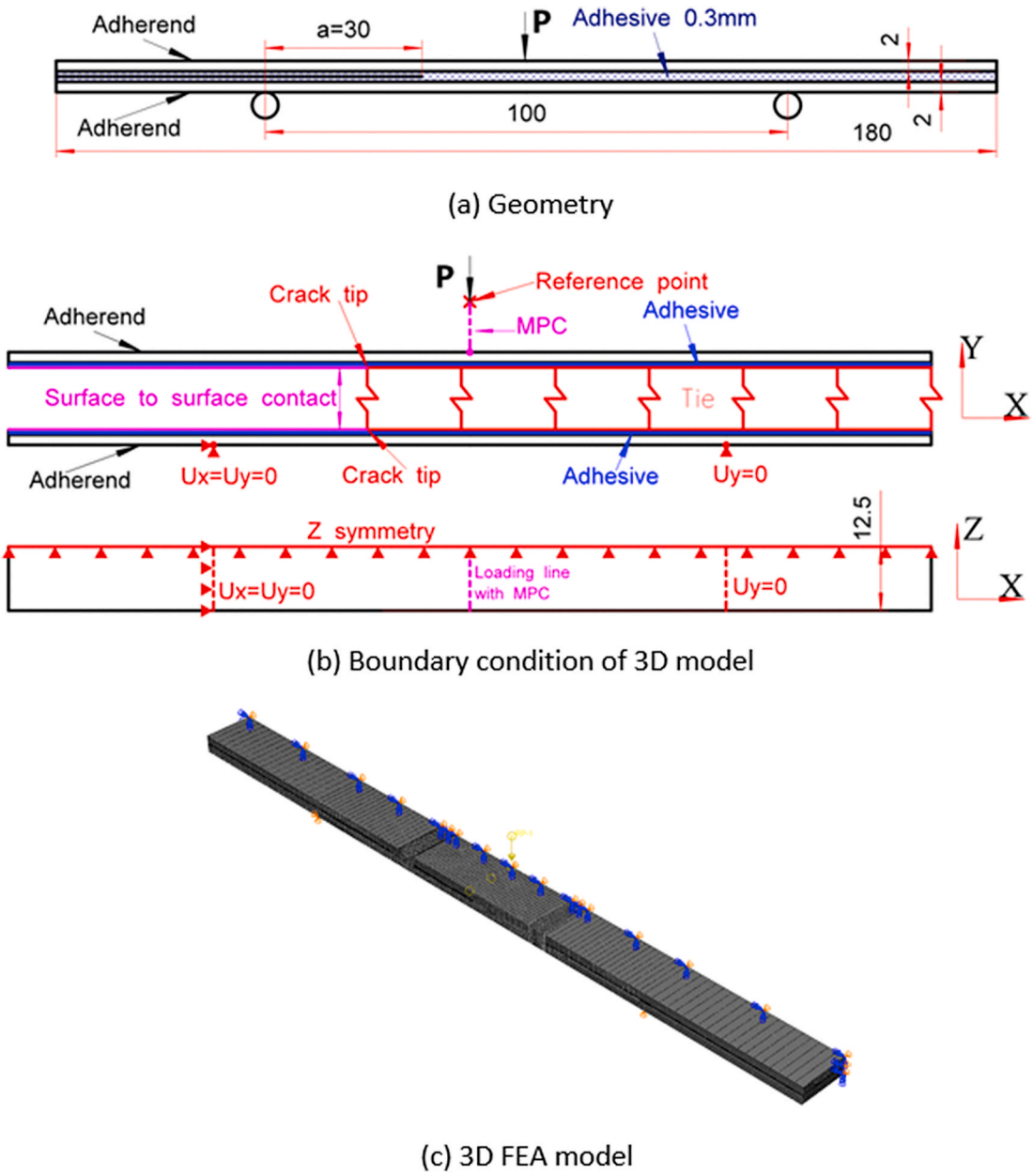

Fig. 17. Geometry and boundary condition of ENF specimen.

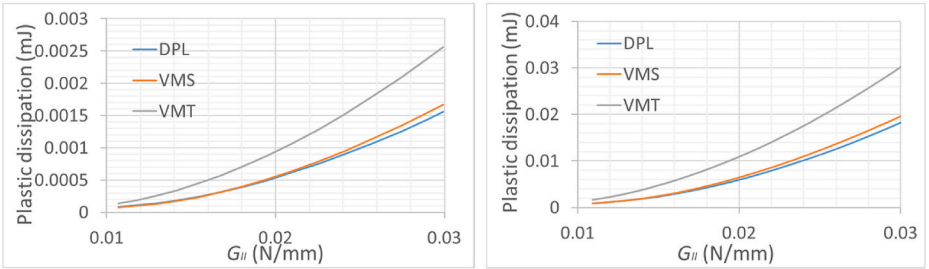

(a) 2D model (b) 3D model

Fig. 18. Plastic dissipation of ENF specimen.

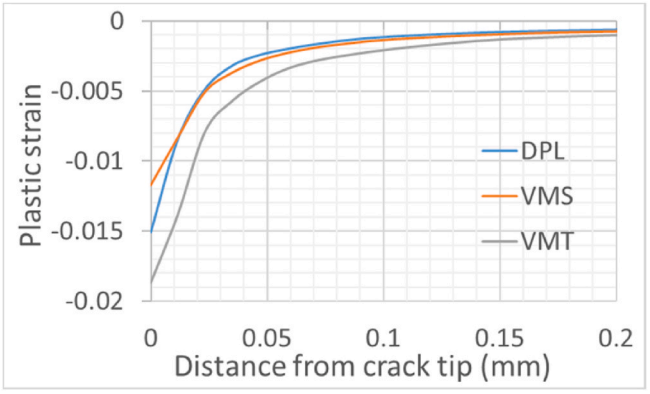

Fig. 19. Plastic strain ε_{xy}^{p} distribution in 2D model.

4.4. Plate with crack bonded repaired under tension

The adhesively bonded repairs are used in aerospace engineering, so the last example focuses on a 2024-T3 plate with a straight through edge crack which is bonded repaired by a patch under tensile loading as shown in Fig. 20. The thickness of adhesive layers is 0.15 mm.

The simulation is in a ½ model for the symmetrical boundary condition in X direction in the area without crack. The crack surface is represented by a free surface. On the left surface the displacement in Y and Z direction are constrained, and an MPC constraint is used between left surface and a reference point to keep the same displacement in X direction. The simulation is force controlled with the load applied on the reference point. The FEA model contains 3 separate parts standing for the plate, adhesive and repair respectively. The part for adhesive is tied to both the part for plate and the part for repair. The 3D 8-node reduced integration element with enhanced hourglass control is used and the part for adhesive is meshed with 75*50*6 elements. In the simulation, the plate with crack bonded repaired by 2024-T3 and composites were both simulated, for aluminum alloy and composites are often involved in bonded repairs. The CFRP is unidirectional with fiber in the X direction. The material property of CFRP is from Ref. [23]: $E_{11} = 135$ GPa, $E_{22} = 10$ GPa, $G_{12} = G_{23} = G_{31} = 5$ GPa, $\nu_{12} = 0.309$ and $\nu_{31} = \nu_{32} = 0.02049$. The FEA model is shown in Fig. 20(c).

The stress field in the adhesive material in the crack tip vicinity is complex, because it subjects to tension from the applied loading and shear from the plate. The stress and strain distribution along path A-B (indicated in Fig. 20) in the first layer of adhesive next to aluminum alloy plate and crack was selected for comparison. Figs. 21 and 22 show the normal stress S_{xx} and normal plastic strain ε_{xx}^{p} distribution in X direction at the load 2.5 kN. Point A is 0 mm in X-axis and Point B is 10 mm in X-axis.

From these figures it is clear that the simulation results with the Von Mises model disagree with the results with DPL regardless of the materials for repair, for the hydrostatic pressure is high around the crack. The high hydrostatic pressure is from the tension in X direction caused by the crack opening. The high hydrostatic pressure influences the plastic behavior of adhesive materials. Therefore, the Von Mises model is not recommended to be used in simulating the adhesive material property in the situations similar to this example with a complex stress field caused by the crack in the plate which is connected by adhesive materials.

5. Conclusion

Quasi-static tests under tensile and shear conditions were performed for measuring the stress-strain relationships of the film adhesive material FM94. The Drucker-Prager model was used in the simulation of pure tension and pure shear to reproduce the material property. Those

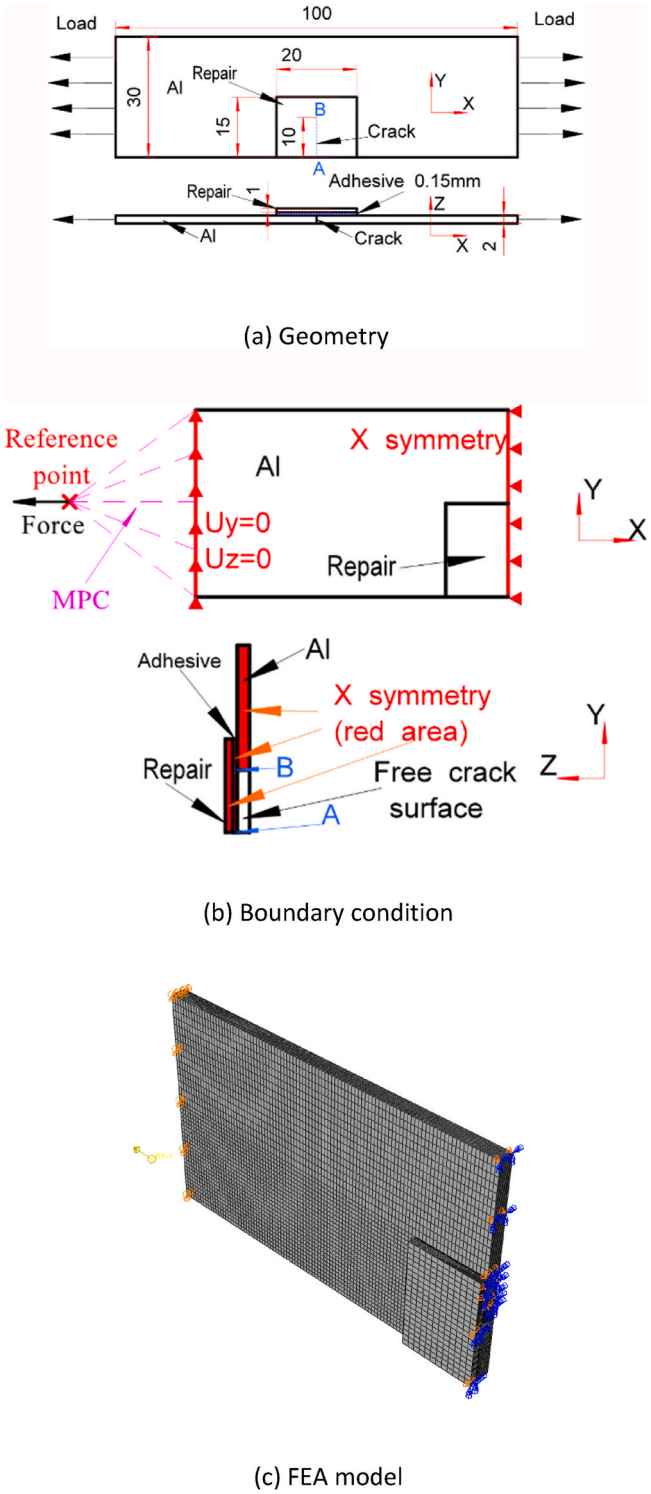

Fig. 20. Plate with crack bonded repaired under tension.

numerical results show good agreement with all experimental data.

A selection of simulation examples commonly used in assessment of engineering structures with adhesive bonded joint was presented to demonstrate the differences caused by different plasticity models. The simulation results with the Von Mises model differ clearly from the simulation results with the Drucker-Prager model. Although individual cases can be described with the Von Mises model if either tensile or shear data is used for input, the Von Mises model lacks generic application to all cases. This is attributed to the effect of hydrostatic pressure on

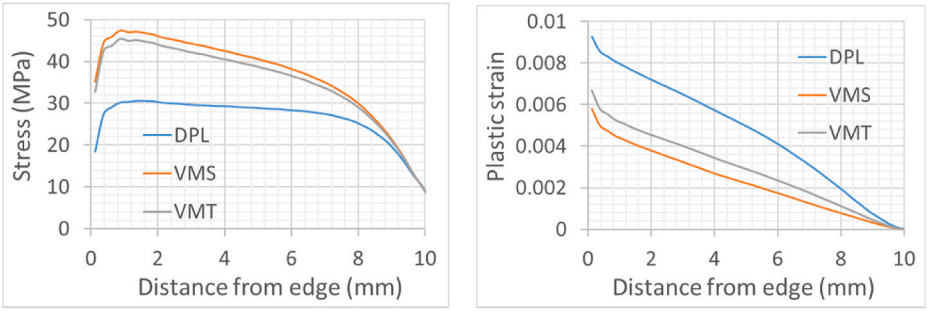

Fig. 21. Stress and strain distribution for bonded repaired by 2024-T3.

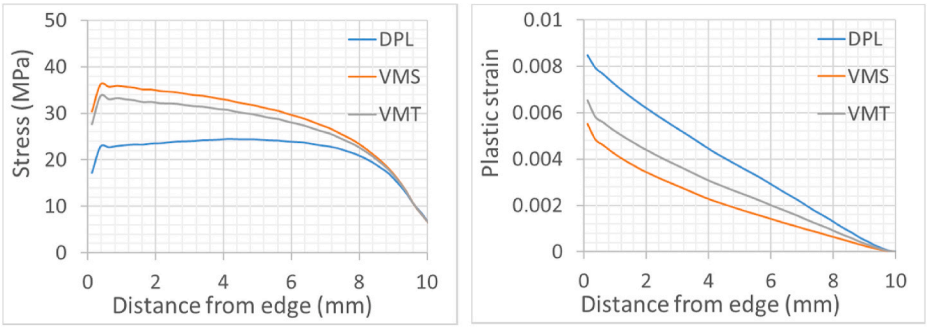

Fig. 22. Stress and strain distribution bonded repaired by CFRP.

yielding, which the Drucker-Prager model does take into account, but the Von Mises model neglects. Therefore, the Drucker-Prager model is more generically applicable for simulating the FM94 material behavior in this paper compared to the Von Mises model. Hence, it is not always correct to use the Von Mises model to simulate adhesive materials under complex loading conditions, in particular in case where the effect of hydrostatic pressure is dominant.

It is undeniable that current work is within a certain scope. The adhesive material property is rate-dependent, while in the experimental work, all the tests were performed under quasi-static condition, so the effect of strain rate was neglected. Further experimental and simulation work at different rates should be done in the future to extend the scope of current work.

References

[1] Chiminelli A, Breto R, Jiménez MA, Velasco F, Abenojar J, Martínez MA. Experimental method for the determination of material parameters of plasticity models for toughened adhesives. Int J Adhesion Adhes 2016;68:182–7.
[2] García JA, Chiminelli A, García B, Lizaranzu M, Jiménez MA. Characterization and material model definition of toughened adhesives for finite element analysis. Int J Adhesion Adhes 2011;31(4):182–92.
[3] Wang Chun H, Peter Chalkley. Plastic yielding of a film adhesive under multiaxial stresses. Int J Adhesion Adhes 2000;20(2):155–64.
[4] ASTM D638-14. Standard test method for tensile properties of plastics. West Conshohocken, PA: ASTM International; 2014.
[5] ASTM D5656-10(2017). Standard test method for thick-adherend metal lap-shear joints for determination of the stress-strain behavior of adhesives in shear by tension loading. West Conshohocken, PA: ASTM International; 2017.
[6] ISO EN. Determination of Shear Behaviour of Structural Adhesives-Part 1: torsion test method using butt-bonded hollow cylinders. 1996. 11003-1.
[7] Derewonko A, Godzimirski J, Kosiuczenko K, Niezgoda T, Kiczko A. Strength assessment of adhesive-bonded joints. Comput Mater Sci 2008;43(1):157–64.
[8] Sayman O. Elasto-plastic stress analysis in an adhesively bonded single-lap joint. Compos B Eng 2012;43(2):204–9.
[9] Al-Ramahi, Nawres J, Roberts Joffe, Varna Janis. Investigation of end and edge effects on results of numerical simulation of single lap adhesive joint with non-linear materials. Int J Adhesion Adhes 2018;87:191–204.
[10] Kupski J, de Freitas ST, Zarouchas D, Benedictus R. On the influence of overlap topology on the tensile strength of composite bonded joints: single overlap versus overlap stacking. Int J Adhesion Adhes 2020;103:102696.
[11] Papanicolaou GC, Charitidis P, Mouzakis DE, Karachalios E, Jiga G, Portan DV. Experimental and numerical investigation of balanced Boron/Epoxy single lap joints subjected to salt spray aging. Int J Adhesion Adhes 2016;68:9–18.
[12] Dean G, Crocker L, Read B, Wright L. Prediction of deformation and failure of rubber-toughened adhesive joints. Int J Adhesion Adhes 2004;24(4):295–306.
[13] Zgoul M, Crocombe AD. Numerical modelling of lap joints bonded with a rate-dependent adhesive. Int J Adhesion Adhes 2004;24(4):355–66.
[14] Özer Halil, Öz Özkan. The use of the exponential Drucker-Prager material model for defining the failure loads of the mono and bi-adhesive joints. Int J Adhesion Adhes 2017;76:17–29.
[15] de Castro Julia, Keller Thomas. Ductile double-lap joints from brittle GFRP laminates and ductile adhesives, Part II: numerical investigation and joint strength prediction. Compos B Eng 2008;39(2):282–91.
[16] Raghava Ram, Caddell Robert M, Yeh Gregory SY. The macroscopic yield behaviour of polymers. J Mater Sci 1973;8(2):225–32.
[17] Jokinen Jarno, Wallin Markus, Saarela Olli. Applicability of VCCT in mode I loading of yielding adhesively bonded joints—a case study. Int J Adhesion Adhes 2015;62:85–91.
[18] Ameli A, Azari S, Papini M, Spelt JK. Crack path selection in the fracture of fresh and degraded epoxy adhesive joints. Eng Fract Mech 2011;78(9):1986–2003. 2011.
[19] Azari S, Papini M, Spelt JK. Effect of adhesive thickness on fatigue and fracture of toughened epoxy joints–Part II: analysis and finite element modeling. Eng Fract Mech 2011;78(1):138–52.
[20] Donough MJ, Gunnion AJ, Orifici AC, Wang CH. Plasticity induced crack closure in adhesively bonded joints under fatigue loading. Int J Fatig 2015;70:440–50.
[21] Pascoe JA, Zavatta N, Troiani E, Alderliesten RC. The effect of bond-line thickness on fatigue crack growth rate in adhesively bonded joints. Eng Fract Mech 2020;229:106959.
[22] Ducept F, Davies P, Gamby D. An experimental study to validate tests used to determine mixed mode failure criteria of glass/epoxy composites. Compos Appl Sci Manuf 1997;28(8):719–29.
[23] Alkhatib F, Mahdi E, Dean A. Crushing response of CFRP and KFRP composite corrugated tubes to quasi-static slipping axial loading: experimental investigation and numerical simulation. Compos Struct 2020;246:112370.